The Astrophysical Journal, 770:144 (9pp), 2013 June 20 doi:10.1088/0004-637X/770/2/144

SOLVING THE NON-BORN–OPPENHEIMER SCHRÖDINGER EQUATION FOR THE HYDROGEN MOLECULAR ION WITH THE FREE COMPLEMENT METHOD. II. HIGHLY ACCURATE ELECTRONIC, VIBRATIONAL, AND ROTATIONAL EXCITED STATES

Hiroyuki Nakashima[1,3], Yuh Hijikata[2], and Hiroshi Nakatsuji[1,3]
[1] Quantum Chemistry Research Institute, JST, CREST, Kyodai Katsura Venture Plaza 107, Goryo Oohara 1-36, Nishikyo-ku, Kyoto 615-8245, Japan; h.nakashima@qcri.or.jp, h.nakatsuji@qcri.or.jp
[2] Fukui Institute for Fundamental Chemistry, Kyoto University, Kyoto 606-8103, Japan
Received 2013 March 22; accepted 2013 April 29; published 2013 June 5

ABSTRACT

Highly accurate wave functions of the ground and electronic ($1s\,\sigma_g$ and $3d\,\sigma_g$), vibrational ($v = 0$–15 for $1s\,\sigma_g$ and $v = 0$–8 for $3d\,\sigma_g$), and rotational ($L = 0$–6: ^1S, ^3P, ^1D, ^3F, ^1G, ^3H, and ^1I) excited states of the hydrogen molecular ion were obtained by solving the non-Born–Oppenheimer (non-BO) Schrödinger equation using the free complement (FC) method. The vibronic states belonging to the electronic excited state $3d\,\sigma_g$ are embedded in the continuum of the dissociation, $H(1s) + H^+$. Nevertheless, they exist as physical bound states that have negligible coupling with the continuum. The complex scaled Hamiltonian was employed to analyze the bound and/or resonance natures of the obtained eigenstates, and a new resonance state appeared between the above two electronic states. We numerically proved that the FC method is a reliable theoretical tool for investigating non-BO quantum effects, and it should be available for various studies of hydrogen-related space chemistry and low-temperature physics.

Key words: astrochemistry – hydrodynamics – ISM: clouds – ISM: molecules – molecular data

Online-only material: color figures

1. INTRODUCTION

The Born–Oppenheimer (BO) approximation (Born & Oppenheimer 1927) provides information that makes it easier to understand chemical problems with potential energy curves. The quantum effect of nuclear motion, however, cannot be ignored for physical phenomena such as proton transfers, systems in time-dependent external fields, or very cold molecules (Fukui 1981; Thomas 1969; Bandrauk et al. 2008; Ospelkaus et al. 2010; Fioretti et al. 2004; Dulieu et al. 2011; Carr et al. 2009; Chin et al. 2010; Kuma & Momose 2009; Enomoto & Momose 2005). In space chemistry, hydrogen is the most dominant species in interstellar molecules, and hydrogen-related compounds (such as H_2^+, H_3^+, H_3, H_5^+, and CH^+) are key to the investigation of the material composition in interstellar clouds (Oka 1980, 1992; McCall et al. 1998; Kumada et al. 2006; Cheng et al. 2010; Kumagai et al. 2007; Crabtree et al. 2011, 2011; Dohnal et al. 2012; Kirchner & Bowers 1987; Beuhler & Friedman 1982). Fine infrared and radio spectroscopy, in which the wavelength corresponds to vibrational and/or rotational excitations, is quite important in the identification of interstellar molecules in dense and sparse interstellar clouds, and it is used to study astronomical problems where the quantum non-BO (non-adiabatic) effect is indispensable. However, since most of the important interstellar molecules are ionic and/or unstable on Earth, experimental studies are generally difficult to perform. Recently, experimental techniques in cryogenic science have been extensively developed resulting in a new field of science related to space chemistry (Ospelkaus et al. 2010; Fioretti et al. 2004; Dulieu et al. 2011; Carr et al. 2009; Chin et al. 2010; Kuma & Momose 2009; Enomoto & Momose 2005). Various quantum-mechanical effects clearly occur at an extremely low temperature and precise quantum-mechanical theoretical studies are required to understand these astronomical observations and low-temperature experiments.

Of the above interstellar species, the hydrogen molecular ion H_2^+ is the simplest and is a good candidate for establishing a theoretical method to solve the non-BO Schrödinger equation. H_2^+ is considered to be an intermediate highly reactive molecule in the generation of H_3^+ from H_2 in interstellar reactions (Oka 1980, 1992; McCall et al. 1998), and the non-BO effect should be significant. In our first paper (Paper I; Hijikata et al. 2009) of this series, we performed very accurate non-BO calculations of H_2^+ and its isotopomers (D_2^+, T_2^+, HD^+, HT^+, and DT^+) by the free complement (FC) method. The FC method was proposed by one of the present authors to very accurately solve the Schrödinger equation of atoms and molecules (Hijikata et al. 2009; Nakatsuji & Davidson 2001; Nakatsuji 2000, 2002, 2004, 2005, 2012; Nakatsuji et al. 2007; Nakashima & Nakatsuji 2008; Ishikawa et al. 2012; Nakatsuji & Nakashima 2005). It is applicable not only to the Schrödinger equation in the BO framework, but also to the relativistic Dirac equation and to the non-BO calculation (Hijikata et al. 2009; Nakatsuji & Nakashima 2005). Our theoretical background was summarized in a review article (Nakatsuji 2012), which is a recommended starting point for understanding the FC method that is a key theory of this paper. In current quantum chemistry in which the BO calculations have been extensively studied, there have only been a few theoretical studies for general atoms and molecules based on the non-BO framework (Tachikawa et al. 1998; Nakai 2002; Nakai et al. 2001, 2005; Bochevarov et al. 2004; Viswanathan et al. 2007; Tachikawa 2002; Shigeta et al. 1998; Dufey & Fischer 2001; Jasper et al. 2006; Webb et al. 2002; Kozlowski & Adamowicz 1991, 1993). In contrast, the FC method is based on the Hamiltonian of the given system and can generate a suitable function space even for non-BO systems.

There have been several theoretical studies performed of non-BO H_2^+ systems (Li et al. 2007; Cassar & Drake 2004; Hilico et al. 2000; Taylor et al. 1999; Bishop & Cheung 1977; Bubin et al. 2005; Bednarz et al. 2005). Extremely accurate

[3] Author to whom any correspondence should be addressed.

wave functions of the ground and low-lying vibrational excited states were recently reported by Li et al. (2007) and Cassar & Drake (2004), but at present the most accurate solutions in a variational sense have been described in our first paper of this series (Hijikata et al. 2009), in which the Gaussian harmonic function was employed to represent the vibrational motion efficiently. The higher-level vibrational excited states were also reported by various authors (Hilico et al. 2000; Taylor et al. 1999; Bishop & Cheung 1977; Bubin et al. 2005; Bednarz et al. 2005), and studies with the adiabatic approximation were performed up to the dissociation limit (Handy & Lee 1996; Wind 1965; Beckel & Hansen 1970). However, there have only been a very few studies about the higher rotational excited states and the electronic excited states using the fully non-BO calculations. In the present paper, which follows the first paper in this series (Hijikata et al. 2009), we further compute the electronic excitation, higher vibrational, and rotational excited states of the hydrogen molecular ion with the FC method. All of these states are quite significant for fully understanding the fine spectra of the hydrogen molecular ion (Carrington et al. 1989a, 1989b; Leach & Moss 1995; Koelemeij et al. 2007; Critchley et al. 2003).

The vibronic states belonging to the electronic excited states may be embedded in the continuum of free particles followed by the vibrational levels of the electronic ground state. The question arises whether such embedded bound states are accurately computable. A second question would be whether any useful information corresponding to the potential energy curve can be obtained from the non-BO wave function. In this series, we not only perform highly accurate non-BO calculations with the FC method, we also attempt to answer the above questions and to develop the theory of non-BO calculations so we can apply it to various fields of science. Topics regarding the non-BO potential energy curve will be discussed in a subsequent paper III in this series (Nakashima & Nakatsuji 2013).

2. FREE COMPLEMENT WAVE FUNCTION

Since the theoretical feature of the FC method has been discussed in our previous papers with various applications (Hijikata et al. 2009; Nakatsuji 2000, 2002, 2004, 2005, 2012; Nakatsuji & Davidson 2001; Nakatsuji et al. 2007; Nakashima & Nakatsuji 2008; Ishikawa et al. 2012; Nakatsuji & Nakashima 2005), we only very briefly introduce the essential part of the theory here. This theory is based on the concept that the system's Hamiltonian should contain all of the information for the solutions, both the energy and wave function. Therefore, the exact wave function should be representable as a functional of the Hamiltonian. The iterative complement (IC) wave function, defined as

$$\psi_{n+1} = [1 + C_n g(H - E_n)]\psi_n, \tag{1}$$

is one of the concrete expressions of such a functional of the Hamiltonian H,[4] which is included explicitly in the wave function. It is a recursion formula that is guaranteed to converge to the exact wave function, where C_n and E_n are the variational coefficient and energy at iteration cycle n. In Equation (1), the scaling function g is introduced to avoid the singularity problem associated with the Coulomb potential. The FC method was proposed to accelerate convergence of the IC method. The FC wave function is defined by

$$\psi_{n+1} = \sum_{i=1}^{M_n} c_i^{(n)} \phi_i^{(n)}, \tag{2}$$

where the right-hand side of Equation (1) is expanded into the independent functions $\{\phi_i^{(n)}\}$, called the complement functions. The independent coefficients $\{c_i^{(n)}\}$ are assigned to each complement function. Here, the iteration number n in the IC method is recalled by "order" in the FC method, and the number of functions is called the "dimension" M_n. The unknown coefficients $\{c_i^{(n)}\}$ are variationally determined if the analytical integrations of the matrix elements are possible. An alternative method to determine $\{c_i^{(n)}\}$ is the local Schrödinger equation method, which is based on a sampling procedure and in principle is applicable to any system and function without encountering integration difficulty (Nakatsuji et al. 2007). In the present paper, we employed the first, variational method with the analytical integrations.

Thus, one of the remarkable features of the FC method is that the Hamiltonian can generate an appropriate set of complement functions for the given system, using the initial function satisfying the symmetries and the boundary conditions, and note that the non-BO Hamiltonian contains the nuclear coordinates as an explicit variable as well as the electron coordinates. In the present H_2^+ case, we employed the initial function given by

$$\psi_0 = (1 \pm P_{12})\left[\left[\sum_{j=1}^{J} \exp(-\alpha^{(j)} s) \exp\left(-\gamma^{(j)}\left(R - R_e^{(j)}\right)^2\right)\right] \cdot Y_{L,M}^{l_1,l_2}(\mathbf{r}_1, \mathbf{r}_2)\right], \tag{3}$$

where the Hylleraas-like coordinates $s = r_1 + r_2$, $t = r_1 - r_2$, and $R = r_{12}$ are employed in the same manner as in our previous paper (Hijikata et al. 2009). Here, r_1 is the distance from the electron to the first nucleus, r_2 is the distance from the electron to the second nucleus, and R is the internuclear distance. J is the number of different exponent sets. $Y_{L,M}^{l_1,l_2}(\mathbf{r}_1, \mathbf{r}_2)$ are the solid spherical harmonics (Schwartz 1961) used to represent a total spatial angular momentum, given by

$$Y_{L,M}^{l_1,l_2}(\mathbf{r}_1, \mathbf{r}_2) = (-1)^{l_2 - l_1 - M}\sqrt{2L+1} \cdot r_1^{l_1} r_2^{l_2} \cdot \sum_{m=-\max(-l_1, M-l_2)}^{\min(l_1, M+l_2)} \begin{pmatrix} l_1 & l_2 & L \\ m & M-m & -M \end{pmatrix} \times Y_{l_1,m}(\widehat{\mathbf{r}_1}) Y_{l_2,M-m}(\widehat{\mathbf{r}_2}), \tag{4}$$

where L is the quantum number of total angular momentum and M is its z element. L and M are conserved as a quantum number. Although l_1 and l_2 are not quantum numbers, l_1+l_2 is conserved. $1 \pm P_{12}$ describes the nuclear spin statics originating from fermion or boson particles. Since the proton is a fermion, we use a plus sign for the singlet and a minus sign for the triplet in Equation (3). The rotational mode relates to the nuclear spin statics. For the angular momentum states with even parity (S, D, G, I, ...), the bound (stable) states should be singlets because the spatial wave function is symmetric and the spin state must be antisymmetric. For odd parity states (P, F, H, ...), the stable states should be triplets. Otherwise, the states would become mostly dissociative. We employed the Gaussian

[4] Atomic units (a.u.) were employed everywhere in this paper.

function $\exp(-\gamma^{(j)}(R-R_e^{(j)})^2)$ for the R coordinate to represent the lower harmonic vibrational motions efficiently, where $R_e^{(j)}$ is another nonlinear parameter.

We also employed the same g function as in the previous paper (Hijikata et al. 2009),

$$g = -\frac{1}{V_{Ne}} + \frac{1}{V_{NN}} = \frac{s^2 - t^2}{4s} + R, \tag{5}$$

where V_{Ne} represents the nucleus–electron attraction potential (with nuclear charge $Z = 1$) and V_{NN} is the nucleus–nucleus repulsive potential. The generated wave function has the form

$$\psi = (1 \pm P_{12})\Bigg[\sum_{(a,b,c,j,l_1,l_2)} C_{(a,b,c,j,l_1,l_2)} \cdot s^a t^b R^c \cdot \exp(-\alpha^{(j)} s) \times \exp\left(-\gamma^{(j)}\left(R - R_e^{(j)}\right)^2\right) \cdot Y_{L,M}^{l_1,l_2}(\mathbf{r}_1, \mathbf{r}_2)\Bigg], \tag{6}$$

where both a and c have the values of integers including negative integers. For the present system, however, the functions using negative integers of a are not very significant because the three-particle coalescence is very rare and their functions were neglected. However, negative integers of c would contribute to the representation of the flexibility of the vibrational motion. As for increasing the order, R^c for highly vibrational excited states is automatically generated by Equation (1). Index b only runs over positive (even or odd) integers, including zero. $C_{(a,b,c,j,l_1,l_2)}$ is the unknown coefficient determined with the variational method. Since the Hamiltonian is totally symmetric, the IC process of Equation (1) does not change the angular quantum numbers L, M, and l_1+l_2 in $Y_{L,M}^{l_1,l_2}(\mathbf{r}_1, \mathbf{r}_2)$ from the initial function. For highly angular momentum (rotational) excited states, therefore, we can independently perform the calculations with the different sets of L, M, and l_1+l_2.

3. BORN–OPPENHEIMER REFERENCE CALCULATIONS

Before proceeding to the fully non-BO calculations, it is worthwhile to draw the BO potential energy curves to aid in understanding the non-BO results. The formal exact solution of the BO H_2^+ system was previously proposed many years ago (Baber & Hasse 1935), but it is necessary to obtain numerically accurate results at the various nuclear coordinates R, both for the electronic ground and excited states. We also performed the FC calculations for the BO case (Ishikawa et al. 2012). The initial and g functions used here for σ_g symmetry are given by

$$\psi_0 = (1 + P_{12}) \sum_{i=1}^{4} \exp(-\alpha_i r_1) \tag{7}$$

and

$$g = r_1 + r_2, \tag{8}$$

respectively, where four different exponents ($\alpha_1 = 1$, $\alpha_2 = 1/2$, $\alpha_3 = 1/3$, $\alpha_4 = 1/4$) are employed to represent both the electronic ground and excited states. Figure 1 shows the BO potential energy curves for $1s\,\sigma_g$, $2s\,\sigma_g$, and $3d\,\sigma_g$, whose assignments are derived from the united atom He^+ at the limit $R = 0$. The potential energy curves were described at 0.1 atomic units (a.u., see footnote 4) intervals, from 0.5 to 40 a.u., with $n = 6$ and $M_n = 112$. The $1s\,\sigma_g$ state has a total energy of

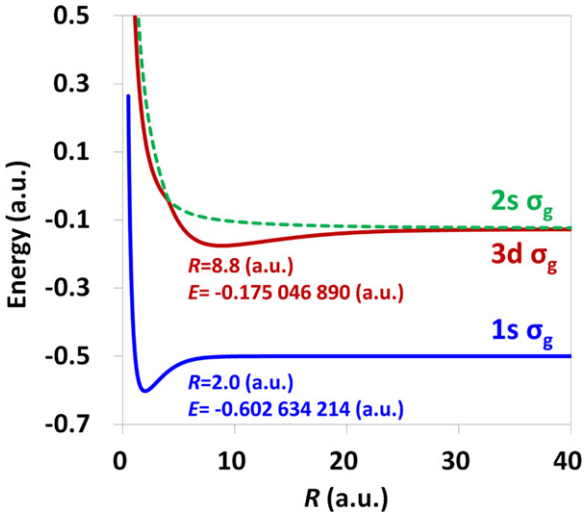

Figure 1. BO potential energy curves of $1s\,\sigma_g$, $2s\,\sigma_g$, and $3d\,\sigma_g$ with $R = 0.5$–40 a.u., calculated by the FC method at $n = 6$ with $M_n = 112$. The equilibrium distance of $1s\,\sigma_g$ was $R_e = 2.0$ a.u. with the energy $E = -0.602\,634\,214$ a.u., and that of $3d\,\sigma_g$ was $R_e = 8.8$ a.u. with the energy $E = -0.175\,046\,890$ a.u.
(A color version of this figure is available in the online journal.)

−0.602 634 214 a.u. (binding energy 2.79 electron volt (eV)) at the equilibrium distance $R_e = 2.0$ a.u. Throughout this paper, the figure that should be correct is shown in bold. Furthermore the precise equilibrium distance was reported as $R_e = 1.997\,193\,320$ a.u. with the total energy of $-0.602\,634\,619\,107$ a.u. (Bishop 1970). The intersystem crossing appears between $2s\,\sigma_g$ and $3d\,\sigma_g$, around $R = 4.0$ a.u. The $2s\,\sigma_g$ state shows a dissociative curve, but $3d\,\sigma_g$ has a minimum with a total energy of **−0.175 046 890** a.u. (binding energy 1.36 eV) at $R_e = 8.8$ a.u. Therefore, the first bound electronic excited state in the σ_g symmetry can be assigned to $3d\,\sigma_g$.

4. ^1S ($L = 0$, $M = 0$) STATES BELONGING TO THE ELECTRONIC GROUND STATE: $1s\,\sigma_g$

Let us begin the fully non-BO calculations of the totally symmetric ^1S ($L = 0$, $M = 0$) states. This paper uses the mass of the proton nucleus, $m_p = 1836.152\,672\,47$ a.u., from NIST 2006.[5] The ψ_0 and g functions of Equations (3) and (5) were used with $(L, M, l_1, l_2) = (0, 0, 0, 0)$ and even parity. To describe both the electronic ground and excited states belonging to the BO states $1s\,\sigma_g$, $2s\,\sigma_g$, and $3d\,\sigma_g$, three different sets of exponents ($J = 3$) were employed,

$$\begin{aligned} &\alpha^{(1)} = 1.0,\ \ \gamma^{(1)} = 4.0,\ \ R_e^{(1)} = 2.0 \\ &\alpha^{(2)} = 0.5,\ \ \gamma^{(2)} = 1.0,\ \ R_e^{(2)} = 8.8 \\ &\alpha^{(3)} = 1/3,\ \ \gamma^{(3)} = 1.0,\ \ R_e^{(3)} = 8.8. \end{aligned} \tag{9}$$

These were estimated by referring to the BO potential energy curves obtained in Section 3. The first set in Equation (9) is for the states belonging to $1s\,\sigma_g$, and the second and third sets are for $2s\,\sigma_g$ and $3d\,\sigma_g$, respectively. These diffuse exponents also help us efficiently describe the highly vibrational excited states.

We performed the calculations up to the order of $n = 15$. Table 1 summarizes the calculated energies of the lowest 16 states corresponding to the vibrational levels $v = 0$–15 (1^1S to 16^1S), at $n = 13$, 14, and 15 with $M_n = 15117$, 18648, and 22689, respectively. Their vibronic states were simultaneously obtained

[5] NIST 2006, see http://physics.nist.gov/cuu/Constants/.

Table 1
The Calculated Energies (a.u.) of the Lowest 16 states (1^1S to 16^1S, $v = 0$ –15) for ^1S ($L = 0$, $M = 0$) Belonging to the Electronic Ground State $1s\,\sigma_g$, with the FC Wave Functions at $n = 13$, 14, and 15 with $M_n = 15117$, 18648, and 22689

State	v	$n = 13$, $M_n = 15117$	$n = 14$, $M_n = 18648$	$n = 15$, $M_n = 22689$	Ref. (1)[a]
1^1S	0	**−0.597 139 063 079 175 256 939 2**58	**−0.597 139 063 079 175 256 939 3**64	**−0.597 139 063 079 175 256 939 379** 108	−0.597 139 063 123 40
2^1S	1	**−0.587 155 679 095 614 799 29**9 648	**−0.587 155 679 095 614 799 300** 529	**−0.587 155 679 095 614 799 300 613**	−0.587 155 679 212 75
3^1S	2	**−0.577 751 904 414 194 306 81**3 623	**−0.577 751 904 414 194 306 819** 170	**−0.577 751 904 414 194 306 819 493**	−0.577 751 904 595 47
4^1S	3	**−0.568 908 498 729 701 336 4**31	**−0.568 908 498 729 701 336 46**2 119	**−−0.568 908 498 729 701 336 463 1**86	−0.568 908 498 966 77
5^1S	4	**−0.560 609 220 848 267 607** 687	**−0.560 609 220 848 267 608 09**7 029	**−0.560 609 220 848 267 608 100 7**62	−0.560 609 221 133 07
6^1S	5	**−0.552 840 749 894 956 8**88	**−0.552 840 749 894 956 906 6**68	**−0.552 840 749 894 956 906 711** 321	−0.552 840 750 219 66
7^1S	6	**−0.545 592 650 992 074** 840	**−0.545 592 650 992 075 29**8 125	**−0.545 592 650 992 075 299 018** 080	−0.545 592 651 349 00
8^1S	7	**−0.538 857 386 965 53**4 819	**−0.538 857 386 965 538 7**84	**−0.538 857 386 965 538 791 94**6 918	−0.538 857 387 347 02
9^1S	8	**−0.532 630 379 354 3**14	**−0.532 630 379 354 320 11**8	**−0.532 630 379 354 320 125 31**4 701	−0.532 630 379 752 64
10^1S	9	**−0.526 910 124 014 2**98	**−0.526 910 124 014 318 4**12	**−0.526 910 124 014 318 467 4**86	−0.526 910 124 421 61
11^1S	10	**−0.521 698 369 012 1**68	**−0.521 698 369 012 238** 530	**−0.521 698 369 012 238 639** 855	−0.521 698 369 420 35
12^1S	11	**−0.517 000 365 276** 605	**−0.517 000 365 276 788** 323	**−0.517 000 365 276 788 88**2 957	−0.517 000 365 677 16
13^1S	12	**−0.512 825 203 143** 532	**−0.512 825 203 143 678** 712	**−0.512 825 203 143 678 95**7 245	−0.512 825 203 527 19
14^1S	13	**−0.509 186 248 36**5 407	**−0.509 186 248 366 53**6 726	**−0.509 186 248 366 539 25**3 249	−0.509 186 248 723 35
15^1S	14	**−0.506 101 680 96**5 848	**−0.506 101 680 967 18**7 952	**−0.506 101 680 967 192 77**2 233	−0.506 101 681 286 51
16^1S	15	**−0.503 595 084 997** 274	**−0.503 595 084 997 88**9 840	**−0.503 595 084 997 892 90**2 790	−0.503 595 085 267 77
Dis.[b]		−0.499 727 839	−0.499 727 839	−0.499 727 839	

Notes.
[a] Proton mass: $m_p = 1836.\,152\,701$ a.u. was used in this reference. This value is different from the value used in the present work.
[b] Dissociation limit ($H(1s) + H^+$) with the finite nuclei.
Reference. (1) Hilico et al. 2000.

by a single diagonalization of the same secular equation. As the orders increased, the energies of all of the vibrational states converged to their exact values and extremely accurate solutions were obtained. However, the ground-state energy was a little worse than the value we reported in our first paper (Hijikata et al. 2009), since the order of the FC method is smaller than the previous one that did not employ diffuse sets of exponents. For the first three vibrational states, the previous results (Hijikata et al. 2009) were variationally the best, even though the ground-state energy has almost 22 digits accuracy at $n = 15$ in the present work. In contrast, the most accurate solutions for the higher vibrational excited states were obtained in the published literature. However, the convergent rates for the higher vibrational states become a little slower than those for the lower states, since the higher order R^c terms, which contribute to the higher vibrational wave functions, are gradually introduced as the order increases.

The electronic ground state of H_2^+ dissociates to $H(1S)$ + H^+ with the internal total energy −0.499 727 839 a.u. while considering the finite nucleus mass effect, where H^+ is considered to be just a free particle. The number of the bound vibronic states lower than the dissociation limit should be finite (Hilico et al. 2000; Wind 1965; Beckel & Hansen 1970). Unfortunately, the present form of the wave function still lacks diffuse functions that sufficiently describe the higher levels very near dissociation. In our subsequent paper in this series (Nakashima & Nakatsuji 2013), we further focus on the more highly vibronic states close to dissociation that have levels experimentally investigated using fine spectroscopy. Their importance is known as an elementary step for capturing the electrons for cold molecules (Critchley et al. 2003).

5. ^1S ($L = 0$, $M = 0$) STATES BELONGING TO THE ELECTRONIC EXCITED STATE: $3d\,\sigma_g$

5.1. Diagonalization of the Real Hamiltonian

In the diagonalization on the symmetry ^1S ($L = 0$, $M = 0$), the vibronic solutions corresponding to the electronic excited states of $3d\,\sigma_g$ are simultaneously obtained with the vibronic states of the electronic ground state. Since the diffuse nonlinear exponents were employed in our initial function (see Equation (9)), the complement functions for the $3d\,\sigma_g$ electronic excited state can be generated efficiently. These states, however, are embedded in the continuum because their energies are higher than the dissociation $H(1S)$ + H^+. In the diagonalization of the real Hamiltonian, unphysical roots that mimic the continuum would appear around the bound physical states. Fortunately, the bound solutions are distinguishable by checking the convergences of the FC wave functions. The energies of the physical bound states correctly converge to some constants (exact values), but the unphysical roots do not converge even if the complement function space becomes enlarged.

Table 2 shows the nine eigenstates, $v = 0$ to 8, denoted by $^e1^1S$ to $^e9^1S$, with $n = 13$, 14, and 15. Their total energies were located above the minimum of the BO $3d\,\sigma_g$ potential curve at $R_e = 8.8$ a.u. All the vibronic states ($^e1^1S$ to $^e9^1S$) smoothly converged and maintained the variational upper bound while the orders increased. Therefore, these vibronic states should be physical and have bounded natures. The energy of the $^e1^1S$ state was very precise with 27 correct digits. Interestingly, this accuracy was better than that of the ^1S state belonging to the electronic ground state, since double diffuse exponents were used. The other vibronic excited states were also quite accurately obtained. The eigenvalues just below $^e1^1S$ were −0.187 278, −0.203 513, and −0.175 924 a.u. at $n = 13$, 14, and 15, respectively. This value does not converge at all and should be an unphysical root. Thus, the vibronic states belonging to the electronic excited states embedded in the continuum could be obtained without any practical difficulty using the FC method. The electronic 0–0 excitation energy between the vibrational ground states of $1s\,\sigma_g$ and $3d\,\sigma_g$ (between 1^1S and $^e1^1S$) was **0.423 172 869 452 689 322 665 212 272 352** 250 a.u. (11.515 eV), which can be accurately compatible with the experiments. There are almost no reports in the literature about the fully non-BO vibronic levels of the electronic excited states, and the present study provides the first accurate calculations for these states. Figure 2 plots all

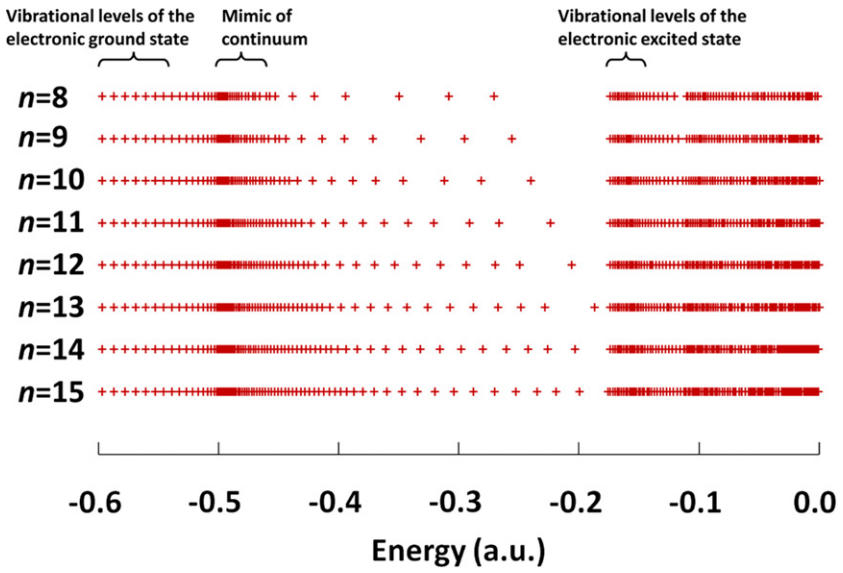

Figure 2. All the eigenvalues calculated at $n = 8$–15 plotted in the region $E = -0.6$ to 0.0 a.u. Each cross point represents the eigenstates of the real Hamiltonian matrix.

(A color version of this figure is available in the online journal.)

Table 2
The Calculated Energies (a.u.) of the Lowest Nine States ($^e1\,^1S$ to $^e9\,^1S$, $v = 0$–8) for ^1S ($L = 0$, $M = 0$) Belonging to the Electronic Excited State $3d\,\sigma_g$, with the FC Wave Functions at $n = 13$, 14, and 15 with $M_n = 15117$, 18648, and 22689

State	v	$n = 13$, $M_n = 15117$	$n = 14$, $M_n = 18648$	$n = 15$, $M_n = 22689$
$^e1\,^1S$	0	**−0.173 966 193 626 485 934 274 166 78**7	**−0.173 966 193 626 485 934 274 166 83**4 277	**−0.173 966 193 626 485 934 274 166 835 64**7 750
$^e2\,^1S$	1	**−0.172 021 711 736 949 357 358 62**5	**−0.172 021 711 736 949 357 358 66**6 630	**−0.172 021 711 736 949 357 358 668 04**1 064
$^e3\,^1S$	2	**−0.170 123 562 006 598 368 2**08	**−0.170 123 562 006 598 368 223** 974	**−0.170 123 562 006 598 368 224 58**7 711
$^e4\,^1S$	3	**−0.168 270 818 426 609 7**97	**−0.168 270 818 426 609 800** 391	**−0.168 270 818 426 609 800 54**1 653
$^e5\,^1S$	4	**−0.166 462 611 337 97**1 602	**−0.166 462 611 337 972 0**34	**−0.166 462 611 337 972 057** 730
$^e6\,^1S$	5	**−0.164 698 126 883 2**12	**−0.164 698 126 883 25**0 016	**−0.164 698 126 883 252 3**68
$^e7\,^1S$	6	**−0.162 976 606 66**2 685	**−0.162 976 606 664** 906	**−0.162 976 606 665 07**1 427
$^e8\,^1S$	7	**−0.161 297 347** 514	**−0.161 297 347 60**5 595	**−0.161 297 347 613** 689
$^e9\,^1S$	8	**−0.159 659 69**9 167	**−0.159 659 701** 760	**−0.159 659 702 04**0 901
Dis.[a]		−0.124 931 959	−0.124 931 959	−0.124 931 959

Note. [a] Dissociation limit ($H(2s) + H^+$) with the finite nuclei.

the eigenvalues in the region, $E = -0.6$ to 0.0 a.u. at $n = 8$–15. As shown above, the physical solutions corresponding to the electronic excited state are distinguishable but the number of unphysical roots rather increases as n becomes large.

5.2. Diagonalization of the Complex-scaled Hamiltonian

To examine the amplitude of the state coupling between the bound states and the continuum, we performed complex scaled calculations (Aguilar & Combes 1971; Balslev & Combes 1971; Simon 1972; Moiseyev 1998; Ehara & Sommerfield 2012; Morita & Yabushita 2008). The complex scaled Hamiltonian for the nonrelativistic Schrödinger equation is generally given by

$$H(\theta) = e^{-2i\theta}T + e^{-i\theta}V, \tag{10}$$

where T and V are the real kinetic and potential operators, respectively, and θ is a rotational angle to the complex plane. The secular equation for the complex Hamiltonian is given by

$$\mathbf{H}(\theta)\mathbf{C}(\theta) = \mathbf{S}\mathbf{C}(\theta)\mathbf{E}(\theta), \tag{11}$$

where $\mathbf{H}(\theta)$ and $\mathbf{S}$ are the complex Hamiltonian and overlap matrices defined as

$$\mathbf{H}_{ij}(\theta) = \langle\phi_i|H(\theta)|\phi_j\rangle, \quad \mathbf{S}_{ij}(\theta) = \langle\phi_i|\phi_j\rangle, \tag{12}$$

and $\mathbf{C}(\theta)$ and $\mathbf{E}(\theta)$ correspond to the complex eigenvectors and eigenvalues which are obtained by solving the complex eigenvalue secular equation, Equation (11). Here, we assume that the basis set (complement function in our case) is independent of θ.

With this formalism, the bound or resonance energies are independent of θ if a complete space is provided. In the actual calculation, however, since a truly complete space cannot be provided, the solutions, even those corresponding to the bound or resonance states, slightly depend on θ. Nevertheless, one can distinguish the bound and resonance states from the continuum and unphysical states, which strongly depend on θ, where the complex eigenvalues rotate according to θ. Table 3 summarizes the complex eigenvalues of the lowest three vibronic states for both the electronic ground and excited states, with $n = 8$ and $M_n = 3918$ at $\theta = 0.04$, 0.08, 0.12, 0.16, and 0.20. Figure 3 plots all the complex eigenvalues in the range $\mathrm{Re}(E(\theta)) = [-0.6,\ 0.0]$ and $\mathrm{Im}(E(\theta)) = [-0.08,\ 0.0]$.

The imaginary eigenvalues of the lower three vibronic states of the $1s\,\sigma_g$ electronic ground state are located in the region 10^{-10} to 10^{-16} at $\theta = 0.04$–0.20, and their real parts were almost independent of θ. As shown in Figure 3, although the lower vibrational excited states are almost located on the real axis, the higher vibronic states rotate to the complex plane

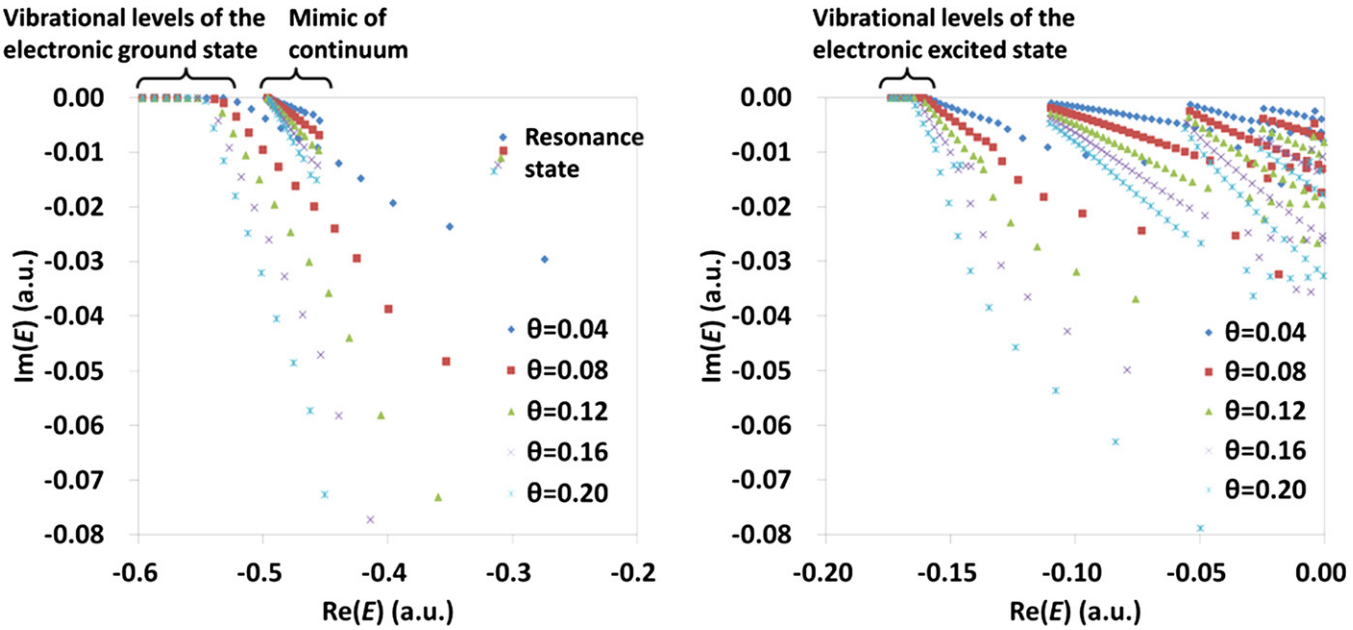

Figure 3. All the complex eigenvalues with $n = 8$ and $M_n = 3918$ at $\theta = 0.04, 0.08, 0.12, 0.16$, and 0.20, plotted to the complex plane in the range $\mathrm{Re}(E(\theta)) = [-0.6,\ 0.0]$ and $\mathrm{Im}(E(\theta)) = [-0.08,\ 0.0]$. The left graph shows the states belonging to the electronic ground state, unphysical roots, and a resonance state. The right graph shows the states belonging to the electronic excited state and other unphysical roots.

(A color version of this figure is available in the online journal.)

Table 3
Complex Eigenvalues (a.u.) of the Theta Dependence of the Low-lying Vibrational States ($v = 0$, 1, and 2) at $n = 8$ with $M_n = 3918$

θ	$v = 0$		$v = 1$		$v = 2$	
	Re(E)	Im(E)	Re(E)	Im(E)	Re(E)	Im(E)
1s σ_g	1^1S		2^1S		3^1S	
0.04	**−0.597 139 063 079 175**	1.56966×10^{-16}	**−0.587 155 679 095 6**29	1.06985×10^{-14}	**−0.577 751 904 41**6 486	1.13922×10^{-12}
0.08	**−0.597 139 063 079 17**3	-7.58710×10^{-16}	**−0.587 155 679 095 6**00	-4.79625×10^{-14}	**−0.577 751 904 41**1 646	-3.05514×10^{-12}
0.12	**−0.597 139 063 079 17**6	6.90623×10^{-15}	**−0.587 155 679 095** 546	1.43139×10^{-13}	**−0.577 751 904 41**5 469	1.05927×10^{-11}
0.16	**−0.597 139 063 079 1**97	-2.57912×10^{-14}	**−0.587 155 679 09**6 479	-1.34969×10^{-13}	**−0.577 751 904 41**8 212	-2.77567×10^{-11}
0.20	**−0.597 139 063 07**8 998	-1.85329×10^{-14}	**−0.587 155 679 09**2 597	-2.58942×10^{-12}	**−0.577 751 904** 319 432	1.00687×10^{-10}
3d σ_g	$^e1^1S$		$^e2^1S$		$^e3^1S$	
0.04	**−0.173 966 193 626 485**	-2.60878×10^{-18}	**−0.172 021 711 736 94**8	-5.32022×10^{-16}	**−0.170 123 562 006** 371	1.92688×10^{-14}
0.08	**−0.173 966 193 626 485**	-1.24321×10^{-17}	**−0.172 021 711 736 94**5	-3.83656×10^{-15}	**−0.170 123 562 00**5 711	1.93559×10^{-13}
0.12	**−0.173 966 193 626 485**	-9.06976×10^{-17}	**−0.172 021 711 736 9**25	-4.69229×10^{-14}	**−0.170 123 56**1 998 005	3.75342×10^{-12}
0.16	**−0.173 966 193 626 48**8	-2.79179×10^{-15}	**−0.172 021 711 736** 582	-7.36512×10^{-13}	**−0.170 123 56**1 813 252	1.32840×10^{-10}
0.20	**−0.173 966 193 626** 717	-5.06931×10^{-13}	**−0.172 021 711** 658 792	-3.48238×10^{-11}	**−0.170 123 5**58 367 653	8.02755×10^{-9}

depending on θ due to the insufficient basis space. From $\mathrm{Re}(E(\theta)) = -0.499\,727$ a.u. (i.e., the exact dissociation limit of H(1s) + H^+), the eigenstates appear on the complex plane with the rotation proportional to θ. Their states should be considered to mimic the continuum, but they are unphysical because there are no continuum basis functions in the present calculations (all of the complement functions have the L^2 boundary condition).

Also, for the lower vibronic states belonging to the $3d\,\sigma_g$ electronic excited state, the imaginary eigenvalues are located in the range 10^{-9} to 10^{-18} at $\theta = 0.04$–0.20, and their real parts were almost independent of θ (see Table 3). At $\theta = 0.02$, the complex eigenvalues of the $^e1^1S$ state for $n = 6$, $M_n = 1806$ and $n = 8$, $M_n = 3918$ were $-0.173\ 966\ 193\ 626 + 2.207\ 052 \times 10^{-17}\ i$ and $-0.173\ 966\ 193\ 626 + 1.018\ 484 \times 10^{-18}\ i$ a.u., respectively. These imaginary parts decrease as the order n increases. In Figure 3, one can also confirm that several lower vibronic states are almost located on the real axis from $\mathrm{Re}(E(\theta)) \approx -0.17$ a.u. Therefore, their states can be considered as bounded states, and there is negligible coupling with the continuum in spite of their being embedded in the continuum. Therefore, the results obtained from the diagonalization of the real Hamiltonian should be sufficiently reliable. In the FC method, we can check the solution convergences with order by order. Only physical roots are independent of the enlargement of the bound complement function space, and the Ritz variational property should hold even for the excited states. The real eigenvalues embedded in the continuum, however, completely mix with the unphysical roots on the real axis. The complex scaled calculation can be used to distinguish the physical states from the unphysical states. Further higher energy solutions shown in Figure 3 are not reliable due to the lack of quality of the wave function.

In Figure 3, one can also notice that a single state exists around $\mathrm{Re}(E(\theta)) = -0.3$ a.u., which is apart from any other unphysical states. This state is not easily recognized in the real Hamiltonian energy spectra because it is completely embedded

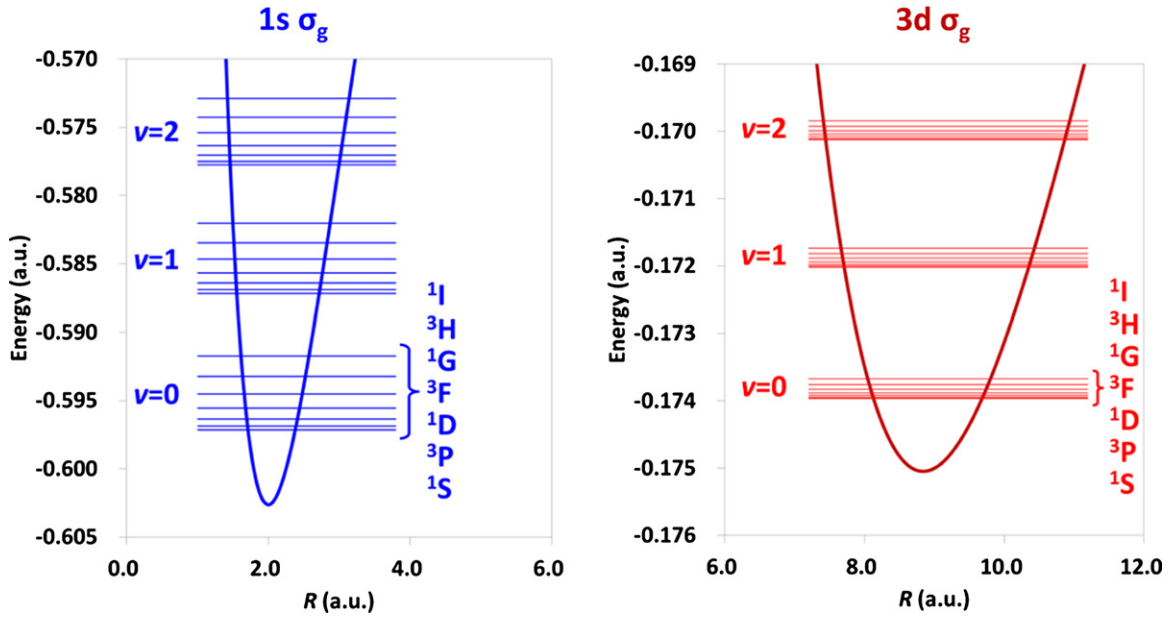

Figure 4. Spectra of the calculated non-BO states of the angular momentum $L = 0$–6 (^1S, ^3P, ^1D, ^3F, ^1G, ^3H, and ^1I states) and vibrational level $v = 0$–2 belonging to the $1s\,\sigma_g$ (left) and $3d\,\sigma_g$ (right) electronic states.

(A color version of this figure is available in the online journal.)

in the continuum and/or unphysical states. However, with the complex scaled Hamiltonian, it is clearly distinguishable with a different nature from the unphysical roots. This state is slightly dependent on θ but that dependency is comparably smaller than those of the other unphysical states. We examined the θ trajectory of the complex eigenvalue at $n = 8$, $M_n = 3918$ and found a single kink point at $-0.307 - 8.80 \times 10^{-3}\,i$ a.u., with an imaginary part non-negligibly larger than any other bound states. Therefore, this state might be a resonance state assigned to the superposition state $H(1s) + H^+ \leftrightarrow H^+ + H(1s)$ in the dissociation process. To discuss this state in detail, however, more accurate calculations are necessary that have a more diffuse basis and/or optimization of the complex exponents (Morita & Yabushita 2008). Since that is not the main purpose of the present paper, we do not discuss this state in depth.

6. HIGHER ANGULAR MOMENTUM (ROTATIONAL EXCITED) VIBRONIC STATES

We also performed calculations for the higher angular momentum vibronic states corresponding to the rotational excitations of $L = 0$–6 (^1S, ^3P, ^1D, ^3F, ^1G, ^3H, and ^1I states). The nuclear spin states are selected as singlets for even L and triplets for odd L; otherwise, they belong to the dissociative σ_u electronic state. In ψ_0 of Equation (3), $Y_{L,M}^{l_1,l_2}(\mathbf{r}_1, \mathbf{r}_2)$ with $(L, M, l_1, l_2) = (L, L, 0, L)$ was employed. The calculations were performed with $n = 6$, except for ^1S, whose calculations were discussed in the above sections. The order $n = 6$ is sufficiently accurate for a direct comparison with experimental data, since even the experimental nuclear mass is only reported up to about 12 digits (see footnote 5).

Table 4 summarizes the total energies of the higher angular momentum states ($L = 0$–6) of the low-lying vibrational states ($v = 0$–2) of both the $1s\,\sigma_g$ and $3d\,\sigma_g$ electronic states. The energy differences ΔE between the two states and the rotational spectra ΔE_r of the rigid body model with the inertia moment I are given by

$$\Delta E_r = \frac{1}{2I}\,[L(L+1) - (L-1)L] \tag{13}$$

and are also listed with units cm^{-1} in Table 4, where $I = \mu R_e^2$ (μ is the reduced mass between two nuclei). Figure 4 illustrates the calculated energy levels for $1s\,\sigma_g$ and $3d\,\sigma_g$ electronic states, respectively, on the BO potential curves.

The energy spacing among the angular momentum states 1^1S–1^3P, 1^3P–1^1D, 1^1D–1^3F, 1^3F–1^1G, 1^1G–1^3H, and 1^3H–1^1I, belonging to the $1s\,\sigma_g$ electronic state and the vibrational level $v = 0$, were 58.232, 116.000, 172.851, 228.257, 282.122, and 333.791 cm^{-1}, respectively. The rotational energy intervals with the rigid body model at $R_e = 2.0$ a.u. were 59.765, 119.530, 179.294, 239.059, 298.824, and 358.589 cm^{-1}, respectively. The former become small as the angular momentum L increases, due to the anharmonicity and non-BO effect. In the rigid body model, the rotational energy intervals are independent of the vibrational level, but in the non-BO calculations, their rotational intervals also become small as the vibrational level increases. The vibrational energy intervals of $1^1S(v = 0)$–$2^1S(v = 1)$ and $2^1S(v = 1)$–$3^1S(v = 2)$ were 2191.100 and 2063.890 cm^{-1}, respectively. Due to the anharmonicity, their difference becomes small for higher vibrational levels.

As already shown in the above section, the electronic 0–0 excitation was 11.515 eV. The energy spacing among the angular momentum states $^e1^1S$–$^e1^3P$, $^e1^3P$–$^e1^1D$, $^e1^1D$–$^e1^3F$, $^e1^3F$–$^e1^1G$, $^e1^1G$–$^e1^3H$, and $^e1^3H$–$^e1^1I$, belonging to the electronic excited state $3d\,\sigma_g$ and the vibrational level $v = 0$, were 3.207, 6.052, 9.074, 12.090, 15.099, and 18.100 cm^{-1}, respectively. Their corresponding rotational energy intervals from the rigid body model were 3.087, 6.174, 9.261, 12.348, 15.435, and 18.522 cm^{-1} with $R_e = 8.8$ a.u. Since R_e is large, their rotational excitation energies are much smaller than those of the electronic ground states. Nevertheless, our non-BO calculations were successful in describing even their small energy differences.

Table 4
Summary of the Non-BO Total Energies at $n = 15$ with $M_n = 22689$ for ^1S and $n = 6$ with $M_n = 2757$, 4167, 5118, 6204, 6915, and 7713 for the ^3P, ^1D, ^3F, ^1G, ^3H, and ^1I States, Respectively

State	Electronic state	v	Energy (a.u.)	ΔE[a] (cm^{-1})	ΔE_r (cm^{-1})
1^1S	$1s\,\sigma_g$	0	**−0.597 139 063 079 175**	...	...
1^3P			**−0.596 873 738 784 2**79	[1^1S–1^3P: R] 58.232	59.765
1^1D			**−0.596 345 205 488** 434	[1^3P–1^1D: R] 116.000	119.530
1^3F			**−0.595 557 638 979** 107	[1^1D–1^3F: R] 172.851	179.294
1^1G			**−0.594 517 169 232** 902	[1^3F–1^1G: R] 228.357	239.059
1^3H			**−0.593 231 728 887** 000	[1^1G–1^3H: R] 282.122	298.824
1^1I			**−0.591 710 864 88**8 091	[1^3H–1^1I: R] 333.791	358.589
2^1S		1	**−0.587 155 679 095 614**	[1^1S–2^1S: V] 2191.100	...
2^3P			**−0.586 904 320 912** 623	[2^1S–2^3P: R] 55.167	59.765
2^1D			**−0.586 403 631 50**4 762	[2^3P–2^1D: R] 109.889	119.530
2^3F			**−0.585 657 611 84**8 892	[2^1D–2^3F: R] 163.732	179.294
2^1G			**−0.584 672 134 09**0 403	[2^3F–2^1G: R] 216.287	239.059
2^3H			**−0.583 454 795 82**2 121	[2^1G–2^3H: R] 267.175	298.824
2^1I			**−0.582 014 736 82**9 357	[2^3H–2^1I: R] 316.056	358.589
3^1S		2	**−0.577 751 904 414 194**	[2^1S–3^1S: V] 2063.890	...
3^3P			**−0.577 514 033** 166	[3^1S–3^3P: R] 52.207	59.765
3^1D			**−0.577 040 234** 350	[3^3P–3^1D: R] 103.987	119.530
3^3F			**−0.576 334 348** 352	[3^1D–3^3F: R] 154.924	179.294
3^1G			**−0.575 401 996** 775	[3^3F–3^1G: R] 204.628	239.059
3^3H			**−0.574 250 472** 910	[3^1G–3^3H: R] 252.730	298.824
3^1I			**−0.572 888 50**7 609	[3^3H–3^1I: R] 298.917	358.589
$^e1^1S$	$3d\,\sigma_g$	0	**−0.173 966 193 626 485**	[1^1S–$^e1^1S$: E] 11.515 eV	...
$^e1^3P$			**−0.173 952 401 595 97**6	[$^e1^1S$–$^e1^3P$: R] 3.027	3.087
$^e1^1D$			**−0.173 924 825 667** 454	[$^e1^3P$–$^e1^1D$: R] 6.052	6.174
$^e1^3F$			**−0.173 883 482 093** 825	[$^e1^1D$–$^e1^3F$: R] 9.074	9.261
$^e1^1G$			**−0.173 828 395 223** 351	[$^e1^3F$–$^e1^1G$: R] 12.090	12.348
$^e1^3H$			**−0.173 759 597 462** 912	[$^e1^1G$–$^e1^3H$: R] 15.099	15.435
$^e1^1I$			**−0.173 677 129 22**3 016	[$^e1^3H$–$^e1^1I$: R] 18.100	18.522
$^e2^1S$		1	**−0.172 021 711 736 949**	[$^e1^1S$–$^e2^1S$: V] 426.764	...
$^e2^3P$			**−0.172 008 199 400** 784	[$^e2^1S$–$^e2^3P$: R] 2.966	3.087
$^e2^1D$			**−0.171 981 182 77**0 821	[$^e2^3P$–$^e2^1D$: R] 5.929	6.174
$^e2^3F$			**−0.171 940 677 92**3 521	[$^e2^1D$–$^e2^3F$: R] 8.890	9.261
$^e2^1G$			**−0.171 886 708 92**8 938	[$^e2^3F$–$^e2^1G$: R] 11.845	12.348
$^e2^3H$			**−0.171 819 307 85**0 269	[$^e2^1G$–$^e2^3H$: R] 14.793	15.435
$^e2^1I$			**−0.171 738 514 60**3 855	[$^e2^3H$–$^e2^1I$: R] 17.732	18.522
$^e3^1S$		2	**−0.170 123 562 006 598**	[$^e2^1S$–$^e3^1S$: V] 416.596	...
$^e3^3P$			**−0.170 110 324 6**29	[$^e3^1S$–$^e3^3P$: R] 2.905	3.087
$^e3^1D$			**−0.170 083 857 9**30	[$^e3^3P$–$^e3^1D$: R] 5.809	6.174
$^e3^3F$			**−0.170 044 177 6**37	[$^e3^1D$–$^e3^3F$: R] 8.709	9.261
$^e3^1G$			**−0.169 991 307 2**30	[$^e3^3F$–$^e3^1G$: R] 11.604	12.348
$^e3^3H$			**−0.169 925 279 5**35	[$^e3^1G$–$^e3^3H$: R] 14.491	15.435
$^e3^1I$			**−0.169 846 130** 566	[$^e3^3H$–$^e3^1I$: R] 17.371	18.522

Notes. The energy differences ΔE between two states and the rotational energy spectra of the rigid model, ΔE_r, are also listed.
[a] E, V, and R denote that the main features of excitation are electronic, vibrational, and rotational excitations, respectively.

Thus, we numerically showed that the present FC method could produce very accurate non-BO wave functions corresponding to all types of the electronic, vibrational, and rotational excited states. Their solutions are considered as the nonrelativistic limit including any coupling of motions. The present theoretical quantum-mechanical study would help in the understanding of the experimental fine spectra of hydrogen molecular ions.

7. CONCLUSION

We performed the fully non-BO calculations of the hydrogen molecular ion as the simplest application of the FC method. The non-BO Hamiltonian includes the electronic, vibrational, and rotational motions, and the exact wave function retains the symmetry of the nuclear spin statics. Accurately solving the non-BO Schrödinger equation is the subject that has not been studied so much as solving the electronic Schrödinger equation within the BO approximation. The FC method can easily handle this subject, since an appropriate potentially exact non-BO wave function is automatically constructed by using the Hamiltonian of the system. This has been numerically proven here by applying it to hydrogen molecular ion.

In the present calculations, accurate electronic, vibrational, and rotational excited states together with the ground state were obtained successfully. The vibronic states belonging to the electronic excited states would be embedded in the continuum. If the state coupling is very small between the physical bound states and the continuum and/or undesired unphysical roots, then the direct diagonalization of the real Hamiltonian is sufficient to obtain their embedded bound solutions. To distinguish the bound

states from the continuum, one may examine the convergent behaviors by increasing the order. An alternative method is to use the complex scaled Hamiltonian, where the undesired continuum and/or unphysical roots rotate in the complex plane with a strong dependence on θ.

The present theoretical study could be used for a direct comparison of experimental studies and astronomical observations. It was also numerically proved that the FC method is a reliable theoretical tool for the precise quantum-mechanical study of the non-BO system. In the subsequent papers in this series (Nakashima & Nakatsuji 2013), we will discuss the potential energy analysis from the non-BO wave function, and we focus on the more highly vibronic or dissociative states close to $H + H^+$ dissociation; this should also be important for fine spectroscopy and low-temperature physics.

This work was supported by JSPS KAKENHI grant No. 24654184. The computations were partially performed in the Research Center for Computational Science, Okazaki, Japan.

REFERENCES

Aguilar, J., & Combes, J. M. 1971, CMaPh, 22, 269
Baber, W. G., & Hasse, H. R. 1935, PCPS, 31, 564
Balslev, E., & Combes, J. M. 1971, CMaPh, 22, 280
Bandrauk, A. D., Chelkowski, S., Kawai, S., & Lu, H. 2008, PhRvL, 101, 153901
Beckel, C. L., & Hansen, B. D., III 1970, JCP, 53, 3681
Bednarz, E., Bubin, S., & Adamowicz, L. 2005, JCP, 122, 164302
Beuhler, R. J., & Friedman, L. 1982, PhRvL, 48, 1097
Bishop, D. M. 1970, JCP, 53, 1541
Bishop, D. M., & Cheung, L. M. 1977, PhRvA, 16, 640
Bochevarov, A. D., Valeev, E. F., & Sherrill, C. D. 2004, MoPh, 102, 111
Born, M., & Oppenheimer, R. 1927, AnAp, 84, 457
Bubin, S., Bednarz, E., & Adamowicz, L. 2005, JCP, 122, 041102
Carr, L. D., DeMille, D., Krems, R. V., & Ye, J. 2009, NJPh, 11, 055049
Carrington, A., McNab, I. R., & Montgomerie, C. A. 1989a, JPhB, 22, 3551
Carrington, A., McNab, I. R., & Montgomerie, C. A. 1989b, CPL, 160, 237
Cassar, M. M., & Drake, G. M. F. 2004, JPhB, 37, 2485
Cheng, T. C., Bandyopadyay, B., Wang, Y., et al. 2010, J. Phys. Chem. Lett., 1, 758
Crabtree, K. N., Kauffman, C. A., Tom, B. A., et al. 2011, JCP, 134, 194311
Crabtree, K. N., Tom, B. A., & McCall, B. J. 2011, JCP, 134, 194310
Critchley, A. D. J., Hughes, A. N., McNab, I. R., & Moss, R. E. 2003, MoPh, 101, 651
Chin, C., Grimm, R., Julienne, P., & Tiesinga, E. 2010, RvMP, 82, 1225
Dohnal, P., Hejduk, M., Varju, J., Rubovič, P., & Roučka, Š. 2012, JCP, 136, 244304
Dufey, F., & Fischer, S. 2001, PhRvA, 63, 042510
Dulieu, O., Krems, R., Weidemüller, M., & Willitschd, S. 2011, PCCP, 13, 18703
Ehara, M., & Sommerfield, T. 2012, CPL, 537, 107
Enomoto, K., & Momose, T. 2005, PhRvA, 72, 061403
Fioretti, A., Fazzi, M., Mazzoni, M., Ban, T., & Gabbanini, C. 2004, PhyS, T112, 13
Fukui, K. 1981, AcChR, 14, 363
Handy, N. C., & Lee, A. M. 1996, CPL, 252, 425
Hijikata, Y., Nakashima, H., & Nakatsuji, H. 2009, JCP, 130, 024102
Hilico, L., Billy, N., Grémaud, B., & Delande, D. 2000, EPJD, 12, 449
Ishikawa, A., Nakashima, H., & Nakatsuji, H. 2012, CP, 401, 62
Jasper, A. W., Mangia, S., Zhu, C., & Truhlar, D. G. 2006, AcChR, 39, 101
Kirchner, N. J., & Bowers, M. T. 1987, JPhCh, 91, 2573
Kozlowski, P. M., & Adamowicz, L. 1991, JCP, 95, 6681
Kozlowski, P. M., & Adamowicz, L. 1993, Chem. Rev., 93, 2007
Kuma, S., & Momose, T. 2009, NJPh, 11, 055023
Kumada, T., Takayanagi, T., & Kumagai, J. 2006, JMoSt, 786, 130
Kumagai, J., Inagaki, H., Kariya, S., Ushida, T., Shimizu, Y., & Kumada, T. 2007, JCP, 127, 024505
Koelemeij, J. C. J., Roth, B., Wicht, A., Ernsting, I., & Schiller, S. 2007, PhRvL, 98, 173002
Leach, C. A., & Moss, R. E. 1995, ARPC, 46, 55
Li, H., Wu, J., Zhou, B.-L., Zhu, J.-M., & Yan, Z.-C. 2007, PhRvA, 75, 012504
McCall, B. J., Geballe, T. R., Hinkle, K. H., & Oka, T. 1998, Sci, 279, 1910
Moiseyev, N. 1998, PhR, 302, 211
Morita, M., & Yabushita, S. 2008, JCoCh, 29, 2471
Nakai, H. 2002, IJQC, 86, 511
Nakai, H., Hoshino, M., & Miyamoto, K. 2005, JCP, 122, 164101
Nakai, H., Sodeyama, K., & Hoshino, M. 2001, CPL, 345, 118
Nakashima, H., & Nakatsuji, H. 2008, PhRvL, 101, 240406
Nakashima, H., & Nakatsuji, H. 2013, PhRvA, submitted
Nakatsuji, H. 2000, JCP, 113, 2949
Nakatsuji, H. 2002, PhRvA, 65, 052122
Nakatsuji, H. 2004, PhRvL, 93, 030403
Nakatsuji, H. 2005, PhRvA, 72, 062110
Nakatsuji, H. 2012, AcChR, 45, 1480
Nakatsuji, H., & Davidson, E. R. 2001, JCP, 115, 2000
Nakatsuji, H., & Nakashima, H. 2005, PhRvL, 95, 050407
Nakatsuji, H., Nakashima, H., Kurokawa, Y., & Ishikawa, A. 2007, PhRvL, 99, 240402
Oka, T. 1980, PhRvL, 45, 531
Oka, T. 1992, RvMP, 64, 1141
Ospelkaus, S., Ni, K.-K., Wang, D., et al. 2010, Sci, 327, 853
Schwartz, C. 1961, PhRv, 123, 1700
Shigeta, Y., Takahashi, H., Yamanaka, S., et al. 1998, IJQC, 70, 659
Simon, B. 1972, CMaPh, 27, 1
Tachikawa, M. 2002, CPL, 360, 494
Tachikawa, M., Mori, K., Nakai, H., & Iguchi, K. 1998, CPL, 290, 437
Taylor, J. M., Yan, Z-C., Dalgarno, A., & Babb, J. F. 1999, MoPh, 97, 25
Thomas, I. L. 1969, PhRv, 185, 90
Viswanathan, B., Barden, C. J., & Boyd, R. J. 2007, JMaCh, 42, 353
Webb, S. P., Iordanov, T., & Hammes-Schiffer, S. 2002, JCP, 117, 4106
Wind, H. 1965, JCP, 43, 2956